PNAS RESEARCH ARTICLE | ECOLOGY
BIOPHYSICS AND COMPUTATIONAL BIOLOGY

Structured foraging of soil predators unveils functional responses to bacterial defenses

Fernando W. Rossine[a,1], Gabriel T. Vercelli[b,1], Corina E. Tarnita[a], and Thomas Gregor[b,c,2]

Edited by Terence Hwa, University of California San Diego, La Jolla; received June 27, 2022; accepted October 23, 2022

Predators and their foraging strategies often determine ecosystem structure and function. Yet, the role of protozoan predators in microbial soil ecosystems remains elusive despite the importance of these ecosystems to global biogeochemical cycles. In particular, amoebae—the most abundant soil protozoan predator of bacteria—remineralize soil nutrients and shape the bacterial community. However, their foraging strategies and their role as microbial ecosystem engineers remain unknown. Here, we present a multiscale approach, connecting microscopic single-cell analysis and macroscopic whole ecosystem dynamics, to expose a phylogenetically widespread foraging strategy, in which an amoeba population spontaneously partitions between cells with fast, polarized movement and cells with slow, unpolarized movement. Such differentiated motion gives rise to efficient colony expansion and consumption of the bacterial substrate. From these insights, we construct a theoretical model that predicts how disturbances to amoeba growth rate and movement disrupt their predation efficiency. These disturbances correspond to distinct classes of bacterial defenses, which allows us to experimentally validate our predictions. All considered, our characterization of amoeba foraging identifies amoeba mobility, and not amoeba growth, as the core determinant of predation efficiency and a key target for bacterial defense systems.

predator–prey | single-cell measurement | modeling

Throughout biomes and across spatial scales—from the vast African savannas to the minute rhizosphere microcosms—foraging strategies are key to how predators shape species diversity and ecosystem function (1). Studies of macroscopic ecosystems have revealed that different aspects of predator foraging strategies—e.g., exploration behavior, dietary selectivity—determine prey encounter rates and the effectiveness of predation deterrents such as plant secondary metabolites (2, 3) or porcupine quills (4). Yet, microbial foraging strategies—in particular, those of soil bacterivore protozoans—remain understudied due to unique challenges: the opacity of soil impedes in loco behavioral observation (5), and metagenomic methods are hindered by the substantial amplification biases in protozoan sequences (6) and the low abundance of protozoan predators relative to their bacterial prey (7). All told, we do not know what strategies soil protozoan predators employ to explore their microscopic landscape, nor do we understand the consequences of such foraging strategies on bacterial population dynamics or on the effectiveness of bacterial defenses.

Thus, characterizing foraging strategies is a crucial missing link to a predictive mechanistic understanding of the well-documented ecological importance of soil protozoan predators, of which amoebae are the most widespread and abundant (8–10). The amoebae are generalist predators that mold soil communities by consuming and limiting bacterial populations (10–12) all the while altering bacterial taxonomic diversity (11, 12). Ultimately, amoebae consume and remineralize a significant portion of the total soil microbial productivity (13, 14), leading to increased nutrient cycling (15, 16). But the consequences of microbial predation go far beyond the soil itself, ranging from changes to biogeochemical cycles to the emergence of pathogens: predator-driven increase of bioavailable nitrogen can fertilize plants (12, 15, 16), remineralized carbon returns to the atmosphere (15), and the interactions between amoebae and fungi are implicated in the evolution of fungal pathogenicity (17).

Amoebae have molecular machinery that enables prey search and handling behaviors required for complex foraging strategies. Amoeba cells can perceive and integrate various cues—mechanical forces (18), temperature (19), and attractant/repellent chemical gradients (20, 21)—leading to oriented cell movement, often toward prey. Once amoebae encounter bacteria, they deploy a lineup of lectins that bind to specific bacteria surface carbohydrates, leading to selective prey handling and consumption (22). When scaled up to thousands of amoebae, such multifactorial behaviors may lead to complex

Significance

Characterization of foraging strategies is crucial to a predictive and mechanistic understanding of the impact that soil protozoan predators—of which amoebae are the most abundant—have on microbial community composition and dynamics. We show that a clonal population of soil amoebae invading a spatially structured bacterial matrix spontaneously differentiates into subpopulations with different types of movement. This strategy determines both the rates of bacteria consumption and the effectiveness of different bacterial antipredator defenses. We further show that such cell behavior differentiation and coordinated movement are conserved, ancestral features of amoebozoans. Since differentiation and coordination are necessary elements of multicellular development, our results suggest that unicellular foraging strategies could have facilitated the multiple independent origins of multicellularity across soil amoebae.

The authors declare no competing interest.

This article is a PNAS Direct Submission.

[1]F.W.R. and G.T.V. contributed equally to this work.

[2]To whom correspondence may be addressed. Email: tg2@princeton.edu.

This article contains supporting information online at http://www.pnas.org/lookup/suppl/doi:10.1073/pnas.2210995119/-/DCSupplemental.

Published December 20, 2022.

emergent features of the predator–prey interaction. Indeed, studies have suggested that amoebae at higher densities consume bacteria more efficiently, pointing toward benefits of collective prey handling (23). The locomotive behavior of a collection of cells may also lead to emergent ecological properties. For instance, experimental and theoretical work on bacteria has shown that the interplay between nutrient consumption and cell movement orientation creates chemical gradients that determine how the bacterial population expands into uncolonized regions (24, 25). Analogously, other studies have suggested that the secretion of chemorepellents might play a role in the expansion of soil amoebae colonies (21, 26). Overall, describing how the behavior of individual amoeba cells results in emergent foraging strategies is fundamental to understanding the efficiency with which amoebae deplete their bacterial prey.

In this study, we identify the foraging strategies that soil amoebae adopt when invading a spatially structured bacterial matrix and show that such foraging strategies determine both the rates of bacteria consumption as well as the effectiveness of different functional classes of bacterial antipredator defenses. We employ a cross-scale approach, characterizing both the microscopic movement patterns of single amoebae within the bacterial matrix and the emergent macroscopic spatial patterns of predation. We first investigate the foraging strategy of *Dictyostelium discoideum*, a well-studied bacterivore soil amoeba species with a complex life cycle comprising a unicellular foraging stage and a multicellular dispersal stage (27). To assess the generality of the observed patterns, we compare *D. discoideum*'s foraging strategy with that of other soil amoebae species with distinct life cycles. In all investigated species, we find cell behavior differentiation and the occurrence of coordinated cell movement. We build a mathematical model that integrates our microscopic and macroscopic observations to make predictions about the macroscopic consequences of disturbing individual cell behaviors. We test these predictions using chemical deterrents that mimic two functional classes of bacterial defenses—predator movement deterrents and predator growth rate deterrents. Altogether, we present an experimental and theoretical framework that quantitatively bridges individual amoeba behaviors and self-organized growth, predator–prey dynamics, and microbial defenses.

Results

Macroscopic and Microscopic Features of Bacterial Matrix Invasion. To elucidate the dynamics of how *D. discoideum* invades the bacterial matrix, we first set out to characterize the macroscopic features of such an invasion. Notably, to ensure that our observations reflect the natural behavior of *D. discoideum* cells, we use natural isolates, rather than the more commonly used lab strains, known for their anomalous colony morphologies (28). We prepared Petri dishes with homogeneous lawns of eGFP-expressing *E. coli* cells grown for 2 d until reaching the stationary phase, by which time the lawns were approximately 100 μm thick, providing a three-dimensional environment for *D. discoideum* cells. At the center of these lawns, we inoculated about 100 cells of *D. discoideum*. These amoeba cells consumed bacteria, divided, and moved within the bacterial matrix, thereby establishing outwardly expanding colonies (Fig. 1*A*). At the border of the colonies, *D. discoideum* cells were present at all depths of the bacterial matrix, although they were predominantly concentrated at the surface of the matrix or in the deeper layers between the matrix and the agar gel (*SI Appendix*, Fig. S1).

Early on, during the bacterial matrix invasion, a highly fluorescent ring develops around the initial *D. discoideum* inoculation zone due to accumulation of bacteria that protrudes above the surface of the bacterial matrix, as can be seen from the confocal images (*SI Appendix*, Fig. S1). It is unclear whether this ring arises from bacterial motion away from *D. discoideum* cells, from the pushing exerted by the advancing *D. discoideum* cells, or from some other process such as increased bacterial growth promoted by *D. discoideum* metabolites. Regardless, this luminous ring demarcates the boundary of the feeding front beyond which amoeba cells are not present. Thus, the luminous ring is used to track the expansion of the nascent amoeba colony (Fig. 1*A*). We find that *D. discoideum* has colony expansion rates of $V_x = 5.2 \pm 0.5\ \mu m/min$ on average. Notably, colonies attain such expansion rates from the moment that the luminous ring becomes visible and before any substantial bacterial consumption occurs (Fig. 1*D*). This is surprising because classical models for expanding populations of isotropically moving cells predict that colony expansion rates should accelerate until the amoeba feeding front stabilizes, which can occur only after bacteria are depleted at the center of the dish (29). This discrepancy between classical models and our observations suggests that anisotropic cell movement might be an important factor in *D. discoideum* colony expansion.

To further characterize the feeding front, we traced radial fluorescence intensity profiles, normal to the colony boundary (*SI Appendix*, Fig. S2 *A* and *B*). Because fluorescence is lost when bacteria are consumed by amoebae (*SI Appendix*, Fig. S2 *C* and *D*), these profile measurements quantify the proportion of consumed bacteria as a function of the distance from the colony boundary. After a transient period lasting up to 2 d, the bacteria consumption profile adopts a constant shape consisting of three distinct zones: the *D. discoideum* colony boundary, which is marked by local accumulation of bacteria; a zone of exponential consumption of bacteria; and a zone exhausted of bacteria (Fig. 1 *B* and *C*). As the colony expands, most *D. discoideum* cells are left behind in the bacteria-depleted zone, whereupon the amoebae transition into starvation-resistant spore cells. To characterize the zone of exponential bacteria consumption, we introduce the halving length ($L_{\frac{1}{2}}$) of the feeding front. It measures the characteristic distance across the feeding front such that the proportion of consumed bacteria falls by half. For *D. discoideum*, we measured halving lengths of $L_{\frac{1}{2}} = 1.5 \pm 0.1$ mm (Fig. 1*E*).

V_x and $L_{\frac{1}{2}}$ provide a temporal and a spatial descriptor, respectively, for the macroscopic characterization of amoeba feeding fronts: V_x reveals how the feeding front advances in time and $L_{\frac{1}{2}}$ reveals how the feeding front is shaped (*SI Appendix*, Fig. S2 *E* and *F*). Importantly, V_x and $L_{\frac{1}{2}}$ are not just descriptors of the feeding front but are also quantities that underlie ecological aspects of the predator–prey interaction: as the bacteria consumption profile stabilizes, V_x sets the global bacteria consumption rate (i.e., the rate at which bacteria are consumed in the entire Petri dish), while $L_{\frac{1}{2}}$ sets the area over which amoeba cells compete for resources by defining the spatial extent of the feeding front.

We next set out to derive the observed macroscopic features of the bacterial matrix invasion from the underlying microscopic organization and dynamics of amoeba cells at the feeding front. To this end, we cut out agar slabs around the feeding front and placed them under a confocal microscope. Infusion of the bacterial lawn with fluorescence (i.e., fluorescein), allows us to track amoeba cells as dark regions within the fluorescent background (Fig. 2 *A* and *B*). At the very boundary of the feeding front, marked by the macroscopically observed luminous ring, amoeba cells accumulate—both at the surface of the bacterial

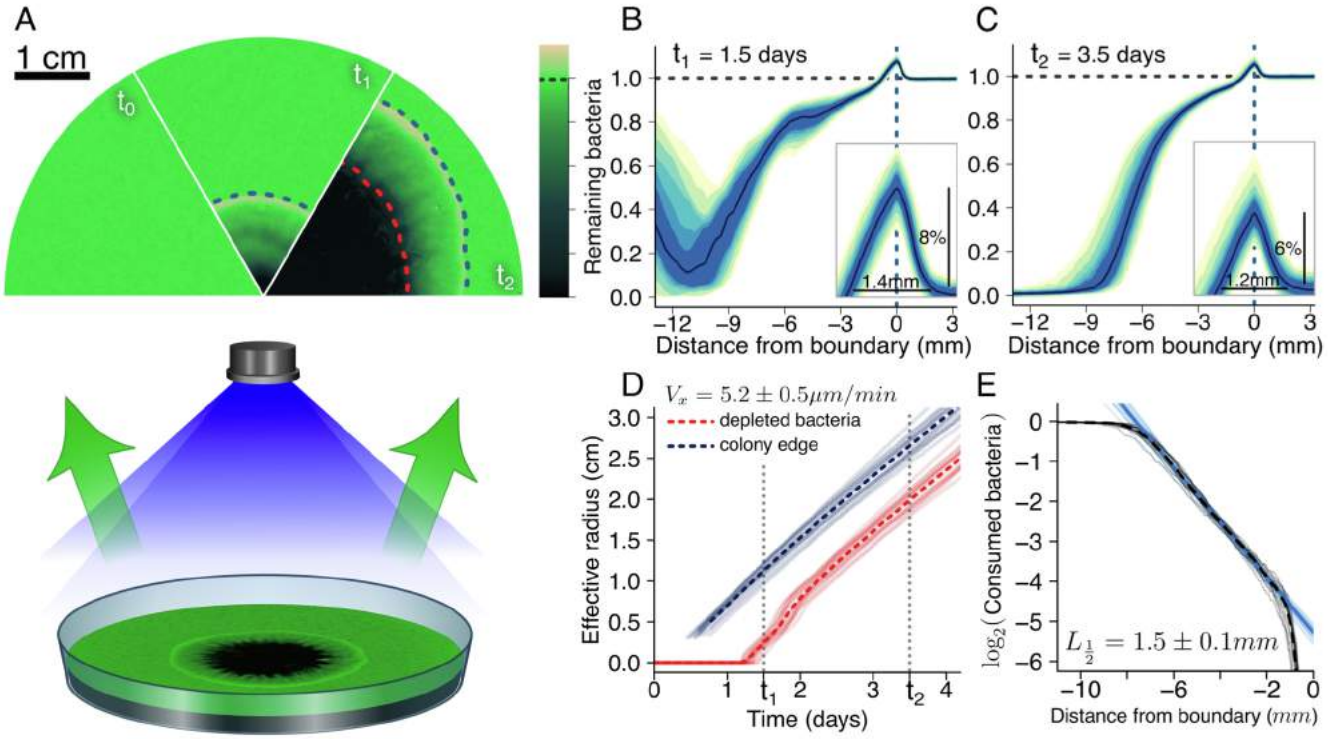

Fig. 1. Macroscopic features of *D. discoideum* invasion: (*A*) Schematic shows a *D. discoideum* colony growing in a bacterial lawn illuminated by a blue LED projector with EGFP-labelled *E. coli* emitting green light. Sectors show the same Petri dish at $t_0 = 0$, $t_1 = 1.5$, and $t_2 = 3.5$ d after amoeba inoculation. The dashed blue line denotes the amoebae colony boundary, and the dashed red line denotes the area of bacterial exhaustion. False color denotes the proportion of remaining bacteria. (*B–E*) Data collected for 16 Petri dishes. (*B–C*) Aggregate profiles of remaining bacteria as a function of distance from the colony boundary for times t_1 (*B*) and t_2 (*C*), each calculated from 40 profiles taken from each of the 16 dishes. Insets show detail of bacterial accumulation along the colony boundary. (*D*) Time courses for the effective radii for both the colony and the depleted bacteria zone. (*E*) Logarithm of consumed bacteria proportion as a function of distance from colony boundary. For (*D* and *E*) transparent lines show time courses for individual dishes, and dashed lines show mean time courses.

matrix and at the interface with the agar gel, while occasionally migrating vertically between the surface and interface—forming a sharp band (Fig. 2*A*). We consider two amoeba cell populations in particular: cells around the boundary of the feeding front (referred to as edge cells) and cells 2.5 mm behind the boundary (referred to as inner cells). Tracking individual cells of these two populations uncovers two strikingly distinct behavioral patterns: inner cells moved in no preferential direction, whereas edge cells displayed markedly polarized trajectories, moving preferentially away from the colony center (Fig. 2 *H* and *I*). To quantify these behavioral patterns, we define a movement polarization coefficient ϕ (see *Methods* and *SI Appendix*, section B.7, Eq. 3) potentially ranging from 0 to 1, for which the edge cells attain $\phi^e = 0.622 \pm 0.004$ and the inner cells attain $\phi^i = 0.010 \pm 0.006$. Moreover, we find that with an average speed of $\bar{v}_e = 3.00 \pm 0.06\,\mu$m/min edge cells move over three times faster than inner cells with $\bar{v}_i = 0.81 \pm 0.01\,\mu$m/min (Fig. 2*C*). Note that the colony expansion rate (V_x) is larger than the average speed of the edge cells ($\bar{v}_e$). This is possible because the colony expansion is influenced not just by the average cell speed but also by the speed of the fastest cells. (We further explain this phenomenon in the following modeling section).

Polarized movement of individual amoeba cells suggests that they respond to some environmental cue (e.g., a bacterially produced chemoattractant, a chemorepellent produced by amoeba cells, or rheological changes to the bacterial matrix caused directly or indirectly by the amoeba cells). Such cues could in fact be responsible for the observed difference between edge- and inner-cell speeds: in many chemotaxis systems both, cell polarization and higher cell speed, arise via a common response to chemical gradients (30, 31). However, it is unclear whether differences in polarization and speed are indeed linked. To test in our system whether cell speed differences persist in the absence of environmental cues, we collect edge cells and inner cells separately, washed them, and placed them in buffer-filled glass bottom dishes. As expected, as cells settled and resumed their pseudopodial motion in this new environment that is devoid of directional cues, cell movement polarization plummeted ($\phi^e_{isol} = 0.017 \pm 0.005$, $\phi^i_{isol} = 0.007 \pm 0.005$). However, edge cells remained faster than inner cells, indicating that some of the behavioral differentiation between inner and edge cells can, at least transiently, persist in the absence of environmental cues (Fig. 2*C*).

The presence of individuals with high and low mobility in the same population is a common pattern in ecology, showing up in species as disparate as sea slugs (32), insects (33), bacteria (30), and even in the multicellular stage of the slime mold life cycle (34). This form of behavioral differentiation often reflects the ubiquitous tradeoff between exploiting local resources and exploring the landscape (35). Given the generality of this tradeoff, it is natural to ask whether other species of soil amoebae would adopt similar bacterial matrix invasion strategies. To investigate this question, we selected another dictyostelid, *Polysphondylium violaceum*, and a more distantly related amoeba species, *Acanthamoeba castellanii*, belonging to the Lobosa group (36). Despite being soil bacterivores, all three of our species of interest are highly divergent and have very different life cycles and cell characteristics. Surprisingly, we find that both *P. violaceum* and *A. castellanii* display the same general macroscopic and microscopic invasion features that we uncovered in *D. discoideum* (*SI Appendix*, Fig. S3). We observe in all species the formation of a broad feeding front demarcated by a bacteria-dense ring, a band of amoeba cells at the colony boundary, and behavioral

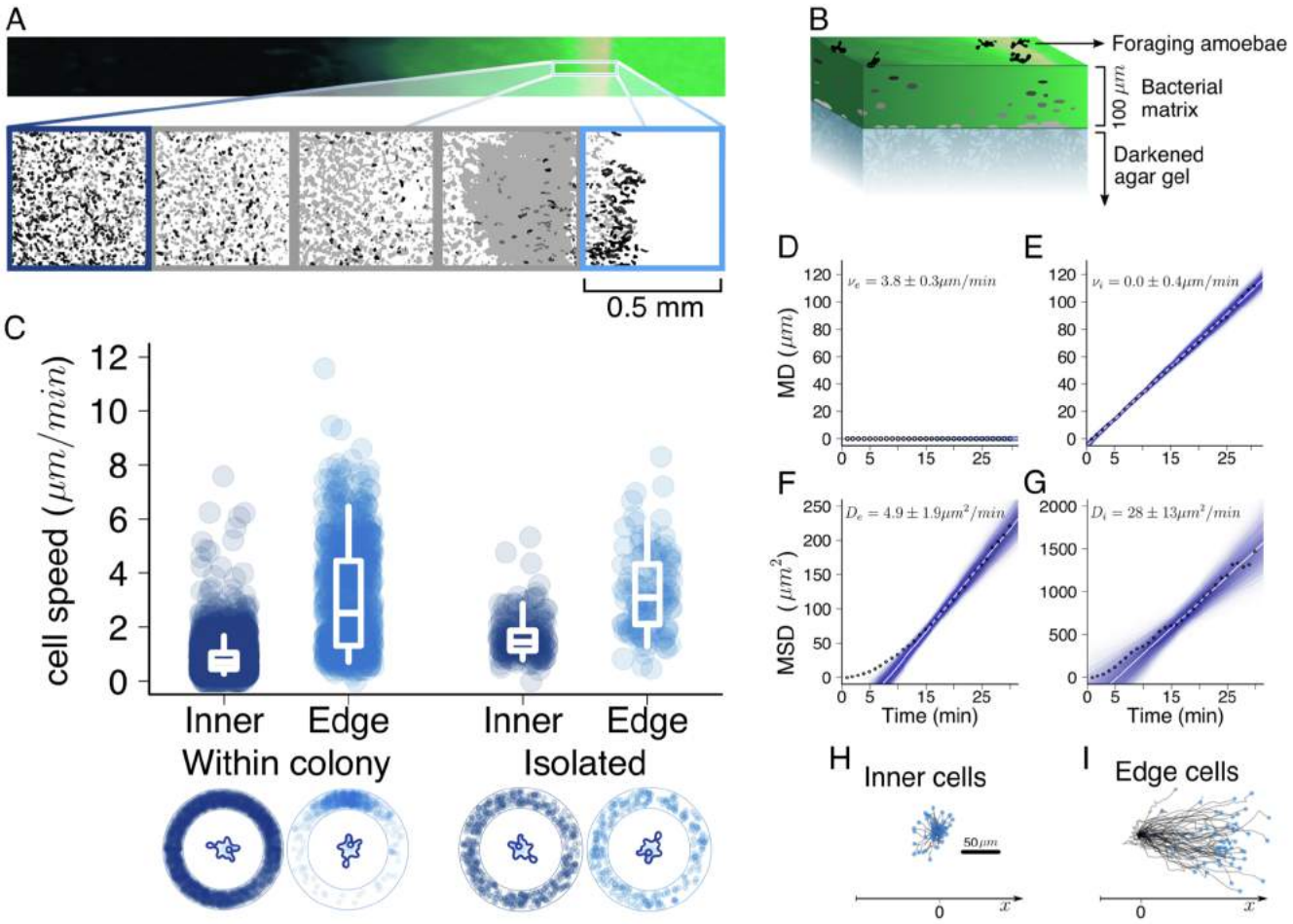

Fig. 2. Microscopic features of *D. discoideum* invasion: (*A*) Region of the feeding front imaged with a confocal microscope. The expanded region shows thresholded confocal images showing *D. discoideum* cells at different depths of the bacterial matrix, with cells shown in black at the surface of the bacterial matrix and cells shown in light gray at the bottom. Each box corresponds to one field of view along the feeding front, ranging from the inner cells (dark blue) to the edge cells (light blue). (*B*) Schematic of the agar slab with the feeding front showing amoeba cells at different depths. (*C*) Median speed (box plots) and direction (ring plots) for individual amoeba trajectories, for inner and edge cells, either embedded in the native feeding front or isolated from the colony. Whiskers of the box plots denote the 5th and 95th percentiles. (*D–G*) Mean amoeba displacement (MD) and mean square displacement (MSD) are shown as a function of time for inner and edge cells. Black points denote data, blue lines are bootstrapped linear regressions (after a relaxation time), and white lines are the median regressions. Advection and diffusion coefficients are respectively calculated as the regression coefficients of the MD and MSD versus time. (*H–I*) Sample trajectories of inner (*H*) and edge (*I*) cells.

differentiation between slow-moving, unpolarized inner cells and fast-moving, polarized edge cells.

A Microscopically Informed Model for Colony Expansion. With both macroscopic and microscopic characterizations of the amoeba colony expansion and bacterial matrix invasion at hand, we are now in a position to ask whether our microscopic description of individual amoeba cell dynamics can explain the macroscopic features of the invasion. In what follows, we will use our microscopic data to build a model that quantitatively predicts the experimentally measured macroscopic outcomes of the bacterial matrix invasion and of the amoebal colony expansion.

We model radial amoeba density $\rho(x, t)$ as a continuous quantity, taking into account cell division and movement, where x is the position measured relative to the amoeba colony boundary b. We assume that amoebae divide at a constant rate r (given as a function of the mean doubling time DT) until bacterial prey is locally exhausted, whereupon cell division halts. We represent amoeba cell movement using a Fokker–Planck operator that consists of an advection term to capture the polarized aspect of cell movement and a diffusive term to capture the dispersive aspect of cell movement (*SI Appendix*). A crucial difference between our model and classical taxis models (24, 25, 31) is our omission of a mechanistic description of cell movement polarization. Instead, as amoebae at different positions of the feeding front have different characteristic movement behaviors (see above), we allow diffusion and advection coefficients to be a function of the distance between the amoebae and the colony boundary. We use our edge cell tracks to extract advection (ν_e) and diffusion (D_e) values for cells around and beyond the colony boundary and our inner cell tracks to extract advection (ν_i) and diffusion (D_i) values for cells in the exponential consumption zone of the feeding front (Fig. 2 *D–I*). Notably, given that inner cell movement is unpolarized, the estimated value for inner cell advection is close to zero (Fig. 2*D*). To obtain advection and diffusion values for the transitional zone (of length l) between the colony boundary and the exponential zone, we interpolate the behavior of edge and inner cells. Following our observation that inner and edge cells retain their differential behaviors even when removed from the feeding front, we introduce a correlation time $\hat{t}$ for which cells retain their movement pattern (*SI Appendix*).

Assuming the existence of a stable invading wave solution, we find analytical relations between the microscopic parameters of the model (i.e., ν_e, ν_i, D_e, D_i, and DT) and the emergent macroscopic feeding front features (i.e., V_x and $L_{\frac{1}{2}}$),

$$V_x = v_e + 2 \cdot \sqrt{\frac{D_e \cdot \log(2)}{\mathrm{DT}}}. \quad [1]$$

$$L_{\frac{1}{2}} = \frac{V_x \cdot \mathrm{DT}}{2} \cdot \left(1 + \sqrt{1 - \frac{D_i \cdot 4\log(2)}{V_x^2 \cdot \mathrm{DT}}}\right). \quad [2]$$

Crucially, these analytical relations are independent of the details and parameters (l, $\hat{t}$) of the behavioral interpolation across the transition zone and independent of K. Therefore, Eq. **1** provides a partitioning of the colony expansion rate into a movement polarization term (v_e) and a cell division–driven term ($2 \cdot \sqrt{\frac{D_e \cdot \log(2)}{\mathrm{DT}}}$), which allows us to estimate that cell growth is contributing to about $26 \pm 9\%$ of the colony expansion rate. We can now employ these relations for an objective criterion to evaluate the performance of our model: We simply require that Eqs. **1** and **2** hold for some combination of parameters within the ranges of our measurements or literature-obtained values.

Using this criterion, we ask whether a single type of cell movement behavior is able to account for the observed macroscopic features. We find that if inner and edge cells all behave in the same way, either all as inner cells or all as edge cells—which we implemented by setting $D_e = D_i$ and $v_e = v_i$—then, the model cannot reconcile our macroscopic and microscopic measurements (*SI Appendix*, Fig. S4 *A* and *B*). However, when we integrate both of the identified cell movement modes into our model, we find good agreement between macroscopic and microscopic measurements (*SI Appendix*, Fig. S4*C*). This implies that the macroscopic patterns of cell expansion cannot be attributed to any particular cell movement mode. Rather, these patterns emerge from the interplay between the distinct edge and inner cell behaviors.

Our model thus recapitulates a series of experimental observations. We find that a narrow region of amoeba cells with polarized movement produces a broad feeding front (Fig. 3*A*), and our microscopic data accurately predicts the expansion rate of this feeding front (Fig. 3*B*). Moreover, by taking our cell movement measurements and macroscopic colony measurements, we employ Eqs. **1** and **2** to estimate cell-doubling times, which fall well within the range found in the literature (Fig. 3*B*). Surprisingly, despite the simplicity of our assumptions about cell movement and cell division, the numerical solutions of our model produce an accumulation of amoeba density at the boundary of the colony (Fig. 3*A*), which correspond to the sharp band of amoebae that we experimentally identified.

To further investigate which factors of cell behavior lead to the formation of the sharp amoeba band, we identified analytical conditions for the existence of such a band in our model. The emergence of the invasion band can be understood as a tug-of-war between edge cell movement and doubling times. Edge cells with faster, more polarized motion—and therefore a higher v_e—favor the formation of the band by separating edge cells from the lagging exponential zone, whereas faster doubling times counteract the separation of the band by increasing cell density along the transitional zone (*SI Appendix*, Fig. S5 *A* and *B*). Parameters describing the transition between edge cell and inner cell behavior also play a role in determining the formation of the invasion band. A narrower transitional zone (smaller l) corresponded to a steeper transition between edge and inner cell behavior, which favors the formation of the band. Furthermore, a longer behavioral switching time $\hat{t}$ leads to increased behavioral variance in the middle of the transitional zone, which also favors the formation of the band (*SI Appendix*, Fig. S5 *C* and *D*).

Finally, we used our model to investigate how disrupting cell behavior leads to changes at the colony level. We consider three types of cell behavior disruption. First, the effect of depolarizing the movement of edge cells which we find should lead to substantially decreased colony expansion rates and narrower feeding fronts (Fig. 3 *A* and *B*). Second, we consider the effect of changing doubling time, both by itself and also in conjunction with depolarizing edge cell movement. Here, we find that, by itself, lengthening of doubling time should not substantially decrease colony expansion rates, instead just broadening the feeding front (Fig. 3 *A*–*C* and *SI Appendix*, Fig. S6). However, if the lengthening of doubling time is coupled to edge cell movement depolarization, an appreciable decrease in colony

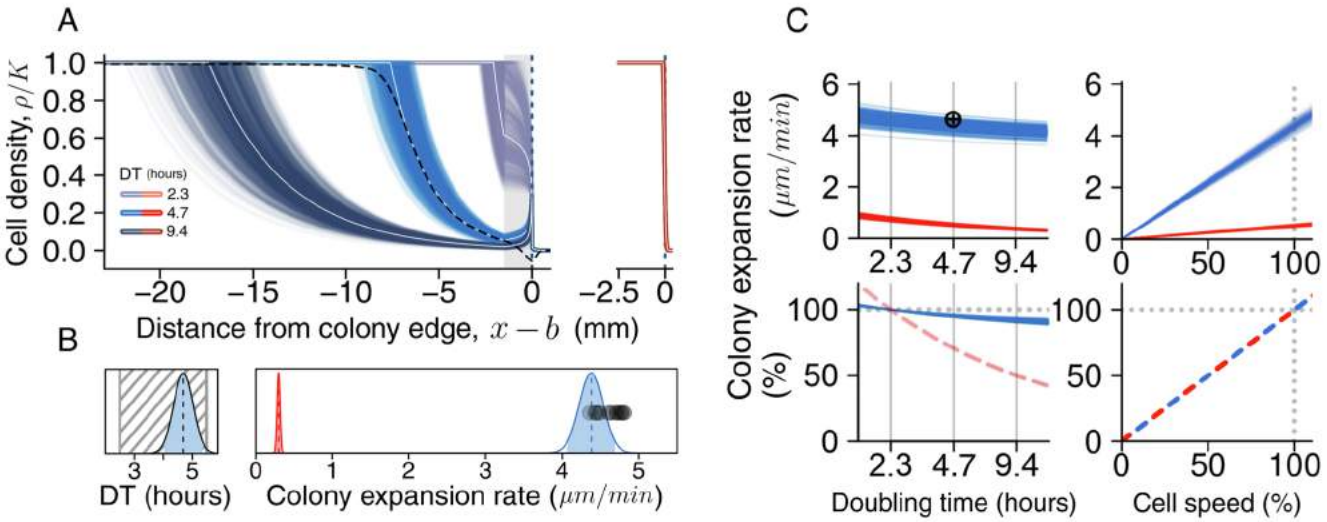

Fig. 3. Modeling colony expansion: (*A*–*C*) Results are shown for the complete model parameterized from microscopic data and accounting for edge cell polarization (in blue) and for a disturbed model, in which the effect of depolarizing the edge cells is observed (in red). (*A*) Numerical realizations of the invading amoeba colony profile produced by our model for the estimated ranges of v_e, D_e, D_i, and a fit K (see *Methods*). White lines show profiles for median estimated parameters. The dashed black line shows data for bacterial consumption. Note that for the depolarized model (in red), all curves collapse regardless of DT. (*B*) The black lined bell curve shows distribution of DT estimated from D_i, V_X, and $L_{\frac{1}{2}}$, and the stripped area shows a literature range for DT. In parallel, V_X is estimated from v_e, D_e, and DT. Black points show measured values for V_X. (*C*) Model-predicted changes to V_X both in absolute terms (first row) or in percentage (second row) as we change cell-doubling time (first column) or cell speed (second column).

expansion rate should occur. Third, we consider the effect of changing cell speed (Fig. 3 *A–C* and *SI Appendix*, Fig. S6) and find that, regardless of edge cell polarization, colony expansion rates should be directly proportional to cell speed (Fig. 3*C*). Altogether, these theoretical results highlight the contribution of edge-cell polarization to the attained colony expansion rate as well as reveal that such movement polarization might buffer the colony expansion rate from increased cell mortality and disrupted cell division.

Disrupting Amoeba Cell Behavior. To probe our theoretical predictions of the colony-level consequences of amoeba cell behavior disruption, we employed toxins that target distinct aspects of amoeba behavior. First, we disrupt cell speed by using nystatin, a toxin naturally produced by the soil-dwelling bacteria *Streptomyces noursei*. Nystatin binds to sterols present in the cell membrane, a common eukaryote-specific target for bacterial toxins, leading to altered cell membrane properties such as increased permeability to ions and increased rigidity (37). Although nystatin causes no detectable mortality to amoeba cells in our experimental conditions (*SI Appendix*, Fig. S7 *A–C*), the speed of individual edge cells is on average $25 \pm 1\%$ slower in the presence of nystatin compared to a control (Fig. 4*A*). Consistent with the theoretical predictions, the diminished cell speed in the experiments containing nystatin results in a $25 \pm 2\%$ slower expansion rate (Fig. 4*B*) as well as in a narrowing of the feeding front (Fig. 4 *C* and *D*).

Second, we sought to independently disrupt *D. discoideum* doubling time by slowing cell division. To this end, we infused our bacterial lawns with 100 μg/mL of fluorouracil, a synthetic uracil analog that acts by inhibiting thymine synthesis to slow down DNA replication and cell division (38). We showed that this concentration of fluorouracil led to a reduction of more than 50% of the growth rate r of *D. discoideum* (*SI Appendix*, Fig. S7*D*). Yet, fluorouracil did not reduce the average cell speed (Fig. 4*E*). Consequently, consistent with our predictions, we observe no reduction in the expansion rates of fluorouracil-treated *D. discoideum* colonies (Fig. 4*F*), in conjunction with a broadening of the feeding front (Fig. 4 *G* and *H*) due to the fluorouracil-induced lengthening of cell-doubling times.

It is worth noting that our analytical results make predictions about only the asymptotic V_x and that although the asymptotic V_x might be relatively unaffected by a reduction in r, the time a *D. discoideum* colony takes to achieve the asymptotic V_x should bear some proportionality to r. However, our experiments indicate that this transient is very short compared to the overall dynamics of bacterial consumption, such that even a doubling of the duration of the transient would still be overall inconsequential. Indeed, from Fig. 1*D*, it can be seen that as soon as the colony is detectable, it is already expanding at full V_x. Overall, our toxin experiments corroborate the distinct theoretically predicted signatures of disrupting cell movement and doubling time.

Toxins might also simultaneously affect both cell movement and doubling times. Although nystatin did not reduce *D. discoideum* viability when cells were embedded in the bacterial matrix (*SI Appendix*, Fig. S7), high mortality is known to occur for amoeba cells directly exposed to buffer with nystatin. Previous work has shown that it is possible to select for *D. discoideum* variants that have lower nystatin-induced mortality, and the resistance mechanism has been linked to membrane sterol compositions with lower nystatin binding (39). Since these resistant variants bind less nystatin, we ask whether the motility effects of nystatin are also diminished in these resistant cells, which could attenuate the reduction in colony expansion rates caused by nystatin.

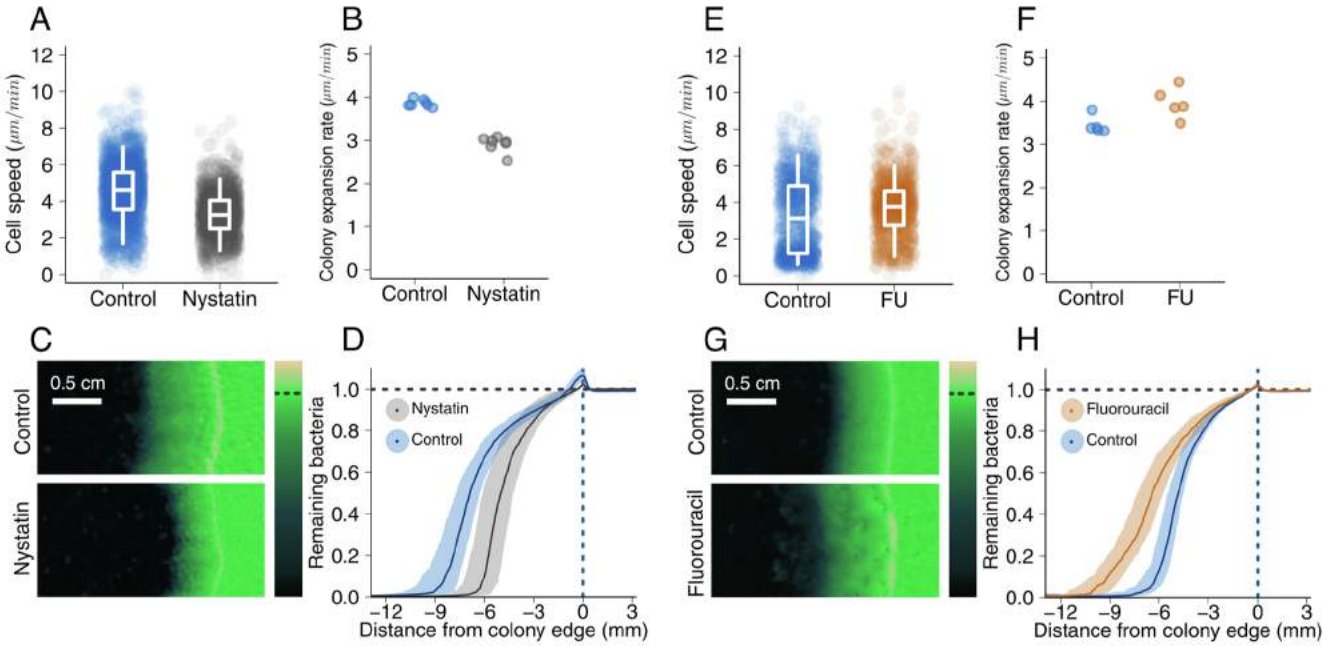

Fig. 4. Toxin-disrupted *D. discoideum* behavior: (*A–D*) Effects of nystatin treatment. (*E–H*) Effects of fluorouracil treatment. (*A* and *E*) Changes to the median speed of single amoeba trajectories for controls and toxin treatments. Whiskers of the box plots denote the 5th and 95th percentiles. One-sided *t*-tests were performed to verify which toxins reduced average cell speed. Nystatin was shown to reduce average cell speed ($P < 0.0000001$), whereas fluorouracil was not ($P = 1$). (*B* and *F*) Resulting differences to colony expansion rates. One-sided *t*-tests were performed to verify which toxins reduced colony expansion rates. Nystatin was shown to also reduce the colony expansion rate ($P = 000001$), whereas fluorouracil was not ($P = 0.98$). (*C* and *G*) Representative images of colonies growing under toxin treatments and controls. (*D* and *H*) Aggregate profiles of remaining bacteria as a function of distance from colony boundary, both under toxin treatments and controls.

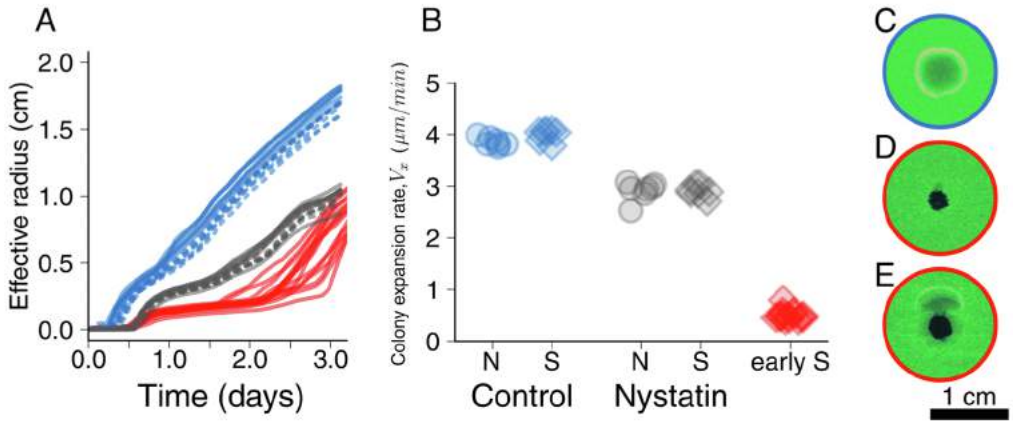

Fig. 5. Properties of nystatin-tolerant colonies: (*A*) Time courses of the effective radius of the bacterial exhaustion zone for *D. discoideum* colonies started from cells that were plated immediately after being selected for nystatin-survival (early S cells, red), nystatin-naive (N) cells grown without nystatin (solid blue lines), N cells grown with nystatin (solid gray lines), and cells selected for nystatin-survival that were allowed to grow in nystatin-infused Petri dishes for three days (S cells) grown with (dashed gray lines) or without nystatin (dashed blue lines). (*B*) Colony expansion rates for the first 2 d of growth. (*C–E*) Representative images of early colony growth for N cells (*C*), early S cells (*D*), and the emergence of naive-like cells in a colony founded by early S cells (*E*, same colony as *D*, but a day later).

We thus repeated our colony expansion experiments with nystatin-resistant amoeba cells, which we selected following previous work (39). Counterintuitively, we find that the nascent colonies seeded from nystatin-survivor cells expand at a much slower rate than those seeded from naive cells, even in the presence of nystatin (Fig. 5 *A* and *B*). This result highlights that in the face of a toxin, the heritable changes (mutations or epigenetic changes) that increase cell viability are potentially distinct—or even conflicting—from the changes that rescue other aspects of cell function such as cell motility, and because cell motility is such an important factor for colony expansion, the more viable cells might turn out to be overall less fit. Moreover, our model predicts that such a reduction to the colony expansion rate should be associated with the loss of the distinct invasion band and a strong steepening of the feeding front (*SI Appendix*, Fig. S5*A*, Fig. 3*A*), which indeed we verify experimentally (Fig. 5 *C* and *D*).

The slowly expanding, nystatin-survivor phenotype cells are potentially at a selective disadvantage when growing alongside naive cells. Accordingly, in the absence of nystatin, we expect a quick loss of resistance. Indeed, a few days into the expansion of colonies seeded with nystatin-survivor cells, small sectors displaying the naive expansion pattern emerge from points around the colony boundary. These naive-like sectors recover the formation of the broad feeding front with the sharp invasion band and eventually take over the entire colony boundary (Fig. 5 *D* and *E*). Subsequently repeating the colony expansion experiments with cells sampled from the naive-like sectors leads to expansion patterns that are indistinguishable from those of colonies seeded with truly naive cells (Fig. 5*A*), suggesting a phenotypic reversal to the naive state.

Altogether, our results indicate that not only does targeting distinct aspects of cell function lead to distinct responses at the colony level but trade-offs can emerge between different aspects of toxin tolerance. Phenotypes that seemingly provide a viability advantage against a toxin might actually underperform when other aspects of cell function, such as motility, are considered.

Discussion

When foraging within the bacterial matrix—a 3D environment with many structural components—the soil-dwelling amoeba *D. discoideum* adopts a spatially structured foraging strategy with faster, polarized edge cells and slower, unpolarized inner cells. This polarization-powered movement strategy gives rise to fast-expanding colonies that develop a sharp ring of explorer cells. Several distantly related soil-dwelling amoeba species all adopt the same general structured movement mode, leading to colonies with ring-like expansion. Curiously, similar ring-like expansion has been identified in phylogenetically and structurally distinct systems, such as bacteria growing in culture media—which also display spatial variation in motility and highly advective edge cells (24). The pervasiveness of this ring expansion pattern is found not only across distinct genera of amoebae but also across different domains of life (Eukaryota and Bacteria), regardless of whether cells move using pseudopods or beating flagellae, over substrates as distinct as culture media or a bacterial matrix. It might be a product of both the ubiquitous trade-off between exploiting local resources and exploring the environment (35) and the energetic efficiency of the underlying spatially differentiated movement modes.

High motility edge cells ensure that the colony will attain a high V_x, while allowing the low motility inner cells to be more energetically efficient without compromising the colony V_x. In the case of amoeba cells, the trade-off between cell motility and energy efficiency is more severe than what would be expected solely due to the direct energetic cost of locomotion—which itself might represent up to half of the cell's respiration (40). Because the same cytoskeletal machinery is required for both pseudopod-based locomotion and endocytosis, faster-moving amoebae pay an opportunity cost in the form of reduced endocytosis, which leads to a reduction of their bacteria intake and biomass accretion to a third of that of slower moving cells (41). An interesting possibility is that the behavioral differences that we observed between inner and edge cells might arise simply by changing the regulation of endocytosis and pseudopod formation. RasS is a protein that is known to be involved in endocytosis regulation, and indeed, *D. discoideum* RasS knockouts were shown to have a higher rate of pseudopod formation relative to the endocytosis rate (41). These mutant lineages display cell speed and polarized morphology very similar to the ones we identified in our wild-type isolated edge cells, suggesting that RasS might be involved in the behavioral differentiation between edge and inner cells. Overall, this observed amoeba cell behavioral differentiation may provide the means to attain a high V_x while limiting the compromise to bacteria consumption.

The emergent colony expansion rate V_x could play an important ecological role in the competition among amoebae for bacterial prey. Amoebae inhabit a dynamic soil environment, in which foraging can occur only during short metabolically active periods following rain or nutrient pulses (9, 10). To persist, amoebae rely on drought-resistant spores that survive and disperse to new bacteria patches during quiescent periods. Amoeba populations compete to produce and disperse these spores. A consequence of this often interrupted life habit is that the consumption of bacteria by amoebae is limited by how fast the amoeba colony can expand before the next dry period. In this context, V_x is likely to affect spore production in two ways: modulating resource consumption and interference with competitors. First, a higher V_x could allow faster-expanding amoeba colonies to consume more bacteria during the short humid periods and thus produce more spores that resist the subsequent drought periods (*SI Appendix*, Fig. S8 *A* and *B*). Secondly, if amoebae co-occur in the same bacteria patch, the ones with a higher V_x may deprive the lower V_x amoebae of these bacterial resources: faster-expanding amoebae physically displace slower-expanding amoebae at the colony boundary (42). This prevents the slower amoebae from accessing bacteria and producing spores (*SI Appendix*, Fig. S8 *A* and *B*). Fast expansion (high V_x) thus both increases one's own dispersal capacity and may also reduce the dispersal capacity of others. The relative contributions of these two competitive modes to overall competition depend on ecological factors, including how often competing types co-occur, the durations of metabolically active and quiescent periods, and the size of bacteria patches. Nevertheless, a higher V_x should always produce a dispersal advantage: higher relative bacteria consumption, more spore production, and consequently higher rates of patch colonization (*SI Appendix*, Fig. S8 *A* and *B*). A challenging but intriguing next step would be to test the ecological importance of V_x in the wild.

From the perspective of the bacterial prey, the ability to resist predator invasion throughout the metabolically active soil periods might result in more bacterial cells that can persist throughout the quiescent periods (spores or otherwise), which would provide a population advantage when conditions improve at the start of a new growth cycle (*SI Appendix*, Fig. S8*C*). Accordingly, bacteria deploy a series of defenses against invading amoebae: structural elements of the bacterial matrix may hamper the advance of invading amoebae (43), changes to bacteria cell shape impede endocytosis (44), and many toxic secondary metabolites are synthesized (45–48). These defenses might act by sterilizing the amoebae and preventing the invasion altogether, by reducing V_x, leading to a decrease in bacteria consumption, or both. However, because the benefit of sterilization without reduction of V_x is substantially conditioned on total predator elimination, such defense strategies are fragile to predator adaptation or evolutionary change. Indeed, different lines of evidence point towards the non-sterilizing character of natural defenses: toxin tolerance varies greatly among different protozoan predators in the same ecosystem (47, 49), the evolution of resistance often occurs in the face of previously sterilizing toxin doses (39), and toxic secondary metabolites are frequently found in the soil in concentrations that are substantially lower than the experimentally characterized minimum inhibitory concentration (45, 50). This suggests that reduction of V_x is an important component of bacterial defenses, and our results imply that bacterial defenses that reduce amoeba doubling time—either by increasing amoeba death rates or decreasing amoeba division rates—lead to a limited reduction of V_x, whereas defenses that target cell motility but that are not necessarily lethal to the predators—as we have shown to potentially be the case for nystatin—achieve a more substantial reduction of V_x.

If, from an ecological perspective, foraging strategies play an important role in microbial predator–prey dynamics, from an evolutionary perspective, these same foraging strategies might have been pivotal to major evolutionary transitions such as the emergence of multicellularity. In particular, dictyostelids have a complex life cycle in which single cells forage until food exhaustion at which point cells aggregate and develop into multicellular fruiting bodies. When first deciphering the mechanisms that allow for cellular aggregation in *D. discoideum*, Bonner proposed that the cellular machinery responsible for tracking food sources might have been repurposed into the multicellularity pathway (20, 27). Although it was later established that dictyostelid signaling pathways were not directly derived from prey chemosensing pathways (51), there is still merit to the general idea that foraging strategies might have provided preadaptations for the emergence of multicellularity. Here, we have shown that two important features of multicellular development, namely the possibility of cell behavior differentiation and the occurrence of coordinated cell movement, are present in the unicellular foraging phase of the dictyostelid life cycle. Moreover, these features are also present in feeding fronts of *Acanthamoebae*, a group that diverged from dictyostelids much earlier than the evolution of the multicellular life cycle. This suggests that some pieces necessary for the coordination of multicellular development are ancestral features of amoebozoans and help shed light on the recurrent and independent appearances of multicellular life forms across soil amoebae.

Materials and Methods

The *D. discoideum* strains NC105.1 from dictybase, *A. castellanii* ATCC 30011 from ATCC, and a locally collected *P. violaceum* were grown in black SM dishes in coculture with *E. coli* bacteria expressing eGFP. Macroscopic images were acquired in a custom-built robot equipped with an EOS Canon camera and a Canon RF 24-105mm f/4-7.1 IS 52 STM lens. Microscopic 45-min videos were obtained by placing agar slabs inside a custom-built moisture chamber around a 20X Zeiss objective (NA 0.8) in a Zeiss LSM 880 confocal microscope. For experiments with Nystatin, the drug was dissolved in DMSO and added to the autoclaved medium for a final concentration of 100 µg/mL. For experiments with fluorouracil, the drug was dissolved in Sor buffer and applied as a mist over fully grown *E. coli* lawns to a final concentration of 100 µg/mL. Image analysis was performed in R, and cells were tracked using ImageJ. Numerical integration of the theoretical model was performed in R using the package deSolve. For more detail on methods and materials, *SI Appendix*.

Data, Materials, and Software Availability. Processed data and analysis code are provided as *SI Appendix*; raw data files and codes are available at https://doi.org/10.34770/5cey-ce46.

ACKNOWLEDGMENTS. We thank Julia Bos and Robert Austin, members of the Gregor and Tarnita labs, and two reviewers for input, support, and suggestions at various stages of the project. F.W.R. and C.E.T. acknowledge support from NSF RoL: FELS: EAGER-1838331. This work was supported in part by the US NSF, through the Center for the Physics of Biological Function (PHY-1734030), and by NIH Grant R01GM097275.

Author affiliations: [a]Department of Ecology and Evolutionary Biology, Princeton University, Princeton, NJ 08544; [b]Joseph Henry Laboratory of Physics, Lewis-Sigler Institute for Integrative Genomics, Princeton University, Princeton, NJ 08544; and [c]Department of Stem Cell and Developmental Biology, CNRS UMR3738, Institut Pasteur, 75015 Paris, France

Author contributions: F.W.R., G.T.V., C.E.T., and T.G. designed research; F.W.R. and G.T.V. performed research; F.W.R., G.T.V., and T.G. contributed new reagents/analytic tools; F.W.R. and G.T.V. analyzed data; and F.W.R., C.E.T., and T.G. wrote the paper.

1. J. A. Estes *et al.*, Trophic downgrading of planet earth. *Science* **333**, 301–306 (2011).
2. G. R. Iason, J. J. Villalba, Behavioral strategies of mammal herbivores against plant secondary metabolites: The avoidance-tolerance continuum. *J. Chem. Ecol.* **32**, 1115–1132 (2006).
3. W. J. Foley, B. D. Moore, Plant secondary metabolites and vertebrate herbivores-from physiological regulation to ecosystem function. *Curr. Opin. Plant Biol.* **8**, 430–435 (2005).
4. T. Katzner, T. A. Miller, J. Rodrigue, S. Shaffer, A most dangerous game: Death and injury to birds from porcupine quills. *Wilson J. Ornithol.* **127**, 102–108 (2015).
5. S. Brethauer, R. L. Shahab, M. H. Studer, Impacts of biofilms on the conversion of cellulose. *Appl. Microbiol. Biotechnol.* **104**, 5201–5212 (2020).
6. S. Geisen *et al.*, Soil protists: A fertile frontier in soil biology research. *FEMS Microbiol. Rev.* **42**, 293–323 (2018).
7. T. W. Crowther *et al.*, The global soil community and its influence on biogeochemistry. *Science* **365** (2019).
8. S. T. Bates *et al.*, Global biogeography of highly diverse protistan communities in soil. *ISME J.* **7**, 652–659 (2013).
9. S. M. Adl, D. C. Coleman, Dynamics of soil protozoa using a direct count method. *Biol. Fertil. Soils* **42**, 168–171 (2005).
10. M. Clarholm, Protozoan grazing of bacteria in soil–impact and importance. *Microb. Ecol.* **7**, 343–350 (1981).
11. K. Rosenberg *et al.*, Soil amoebae rapidly change bacterial community composition in the rhizosphere of *Arabidopsis thaliana*. *ISME J.* **3**, 675–684 (2009).
12. K. Kreuzer *et al.*, Grazing of a common species of soil protozoa (*acanthamoeba castellanii*) affects rhizosphere bacterial community composition and root architecture of rice (Oryza sativa l.). *Soil Biol. Biochem.* **38**, 1665–1672 (2006).
13. P. C. de Ruiter, A. M. Neutel, J. C. Moore, Modelling food webs and nutrient cycling in agro-ecosystems. *Trends Ecol. Evol.* **9**, 378–383 (1994).
14. E. Elliott, D. Coleman, Soil protozoan dynamics in a shortgrass prairie. *Soil Biol. Biochem.* **9**, 113–118 (1977).
15. M. Bonkowski, Protozoa and plant growth: The microbial loop in soil revisited. *New Phytol.* **162**, 617–631 (2004).
16. M. Clarholm, Interactions of bacteria, protozoa and plants leading to mineralization of soil nitrogen. *Soil Biol. Biochem.* **17**, 181–187 (1985).
17. P. Albuquerque *et al.*, A hidden battle in the dirt: Soil amoebae interactions with Paracoccidioides spp. *PLoS Negl. Trop. Dis.* **13**, e0007742 (2019).
18. C. Rivière *et al.*, Signaling through the phosphatidylinositol 3-kinase regulates mechanotaxis induced by local low magnetic forces in *Entamoeba histolytica*. *J. Biomech.* **40**, 64–77 (2007).
19. C. B. Hong, D. R. Fontana, K. L. Poff, Thermotaxis of Dictyostelium discoideum amoebae and its possible role in pseudoplasmodial thermotaxis. *Proc. Natl. Acad. Sci. U.S.A.* **80**, 5646–5649 (1983).
20. J. Bonner *et al.*, Acrasin, acrasinase, and the sensitivity to acrasin in Dictyostelium discoideum. *Dev. Biol.* **20**, 72–87 (1969).
21. J. E. Phillips, R. H. Gomer, A secreted protein is an endogenous chemorepellant in Dictyostelium discoideum. *Proc. Natl. Acad. Sci U.S.A.* **109**, 10990–10995 (2012).
22. T. Farinholt, C. Dinh, A. Kuspa, Microbiome management in the social amoeba Dictyostelium discoideum compared to humans. *Int. J. Dev. Biol.* **63**, 447–450 (2019).
23. M. Rubin *et al.*, Cooperative predation in the social amoebae Dictyostelium discoideum. *PloS One* **14**, e0209438 (2019).
24. J. Cremer *et al.*, Chemotaxis as a navigation strategy to boost range expansion. *Nature* **575**, 658–663 (2019).
25. A. V. Narla, J. Cremer, T. Hwa, A traveling-wave solution for bacterial chemotaxis with growth. arXiv preprint (2021). http://arxiv.org/abs/2103.08100.
26. J. E. Phillips, R. H. Gomer, The ROCO kinase QkgA is necessary for proliferation inhibition by autocrine signals in Dictyostelium discoideum. *Eukaryot. Cell* **9**, 1557 (2010).
27. J. T. Bonner, *Cellular Slime Molds* (Princeton University Press, 2015).
28. P. Fey, R. J. Dodson, S. Basu, R. L. Chisholm, *One Stop Shop for Everything Dictyostelium: Dictybase and the Dicty Stock Center in 2012 in Dictyostelium Discoideum Protocols* (Springer, 2013), pp. 59–92.
29. J. D. Murray, *Mathematical Biology: I. An Introduction* (Springer Science & Business Media, 2007).
30. J. P. Armitage, R. Schmitt, Bacterial chemotaxis: Rhodobacter sphaeroide and Sinorhizobium meliloti-variations on a theme?*Microbiology* **143**, 3671–3682 (1997).
31. E. F. Keller, L. A. Segel, Model for chemotaxis. *J. Theor. Biol.* **30**, 225–234 (1971).
32. P. J. Krug, Not my "type": Larval dispersal dimorphisms and bet-hedging in Opisthobranch life histories. *Biol. Bull.* **216**, 355–372 (2009).
33. D. A. Roff, D. J. Fairbairn, Wing dimorphisms and the evolution of migratory polymorphisms among the insecta. *Am. Zool.* **31**, 243–251 (1991).
34. F. W. Rossine, R. Martinez-Garcia, A. E. Sgro, T. Gregor, C. E. Tarnita, Eco-evolutionary significance of "loners". *PLoS Biol.* **18**, e3000642 (2020).
35. K. Mehlhorn *et al.*, Unpacking the exploration-exploitation tradeoff: A synthesis of human and animal literatures. *Decision* **2**, 191 (2015).
36. T. Cavalier-Smith *et al.*, Multigene phylogeny resolves deep branching of Amoebozoa. *Mol. Phylogenet. Evol.* **83**, 293–304 (2015).
37. L. Silva, A. Coutinho, A. Fedorov, M. Prieto, Competitive binding of cholesterol and ergosterol to the polyene antibiotic nystatin. A fluorescence study. *Biophys. J.* **90**, 3625–3631 (2006).
38. W. Loomis Jr, Sensitivity of Dictyostelium discoideum to nucleic acid analogues. *Exp. Cell. Res.* **64**, 484–486 (1971).
39. D. Scandella, R. Rooney, E. Katz, Genetic, biochemical, and developmental studies of nystatin resistant mutants in Dictyostelium discoideum. *Mol. General Genet. MGG* **180**, 67–75 (1980).
40. D. W. Crawford, A. Rogerson, J. Laybourn-Parry, Respiration of the marine amoeba Trichos-phaerium sieboldi determined by 14 c labelling and Cartesian diver methods. *Mar. Ecol. Prog. Ser.* 135–142 (1994).
41. J. R. Chubb, A. Wilkins, G. M. Thomas, R. H. Insall, The Dictyostelium RasS protein is required for macropinocytosis, phagocytosis and the control of cell movement. *J. Cell. Sci.* **113**, 709–719 (2000).
42. N. J. Buttery *et al.*, Structured growth and genetic drift raise relatedness in the social amoeba Dictyostelium discoideum. *Biol. Lett.* **8**, 794–797 (2012).
43. S. Huws, A. J. McBain, P. Gilbert, Protozoan grazing and its impact upon population dynamics in biofilm communities. *J. Appl. Microbiol.* **98**, 238–244 (2005).
44. K. Jürgens, C. Matz, Predation as a shaping force for the phenotypic and genotypic composition of planktonic bacteria. *Antonie van Leeuwenhoek* **81**, 413–434 (2002).
45. J. M. Raaijmakers, M. Mazzola, Diversity and natural functions of antibiotics produced by beneficial and plant pathogenic bacteria. *Ann. Rev. Phytopathol.* **50**, 403–424 (2012).
46. M. Mazzola, I. De Bruijn, M. F. Cohen, J. M. Raaijmakers, Protozoan-induced regulation of cyclic lipopeptide biosynthesis is an effective predation defense mechanism for pseudomonas fluorescens. *Appl. Environ. Microbiol.* **75**, 6804 (2009).
47. M. Klapper, J. Arp, M. Günther, P. Stallforth, The role of bacterial natural products in predator defense. *Synlett* **29**, 537–541 (2018).
48. M. Klapper, S. Götze, R. Barnett, K. Willing, P. Stallforth, Bacterial alkaloids prevent amoebal predation. *Angew. Chem. Int. Ed.* **55**, 8944–8947 (2016).
49. D. A. Brock, W. É. Callison, J. E. Strassmann, D. C. Queller, Sentinel cells, symbiotic bacteria and toxin resistance in the social amoeba Dictyostelium discoideum. *Proc. R. Soc. B: Biol. Sci.* **283**, 20152727 (2016).
50. A. Jousset, S. Scheu, M. Bonkowski, Secondary metabolite production facilitates establishment of rhizobacteria by reducing both protozoan predation and the competitive effects of indigenous bacteria. *Funct. Ecol.* **22**, 714–719 (2008).
51. O. Shimomura, H. Suthers, J. Bonner, Chemical identity of the acrasin of the cellular slime mold Polysphondylium violaceum. *Proc. Natl. Acad. Sci. U.S.A.* **79**, 7376–7379 (1982).